UNIVERSITÀ DI PISA
Dipartimento di Fisica

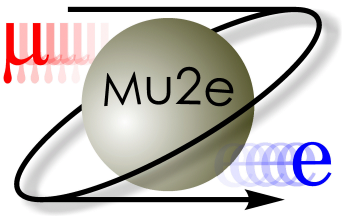

Study of Antiproton Background in the Mu2e Experiment

Giovanni De Felice

Particle Physics Student at Univeristy Of Pisa

Summer Student Programme 2019 at Fermi National Accelerator Laboratory

supervised by
Dr. Robert H. Bernstein

October 10, 2019

Abstract

A new model for antiproton production from protons on heavy nuclei is proposed. With few physical assumptions the new model does the calculation in the center-of-mass and then the variables are boosted back to the laboratory frame. The goal is to predict the antiproton background flux at the beginning of the Transport Solenoid in the Mu2e experiment with this new model. A comparison with the previous model is also needed in order to make a check and to predict changes. With respect to the previous model the new one predicts a lower rate of about a factor 2 for those events produced towards the Transport Solenoid. To conclude, an uncertainty of the order of $\sim 10\%$ is estimated propagating the errors on the fit parameters.

1 Introduction

The Mu2e experiment (Ref. [**1**]), located at Fermilab, will search for charged-lepton flavor violation (CLFV Ref. [**2**]); the process of interest is the neutrino-less conversion of a negative muon into an electron in the field of a nucleus:

$$\mu^- N \longrightarrow e^- N \tag{1}$$

The goal is to improve the previous limit on the conversion rate by four orders of magnitude reaching a 90% CL of $8 \cdot 10^{-17}$. A deep understanding of all the backgrounds is thus essential in order to reach that precision, furthermore, predicted background rates can lead to modifications to the previous design of the experiment. The first step is now to have a good physical model with which to predict the production cross section for every process marked as background.

In this context I studied what concerns the antiproton production comparing a new model proposed by Robert Bernstein with a previous one from Sergei Striganov based on Tan and Ng's model Ref. [**4**] and another from Ying Wang based on Duperray's model Ref. [**5**]. Before going into details it is appropriate to give a very short introduction to the physics behind this search and to the overall Mu2e experiment.

2 Charged-Lepton Flavor Violation

The fermion contribution to the Standard Model, with their masses and mixing among different generations, is described by the Yukawa couplings of the fermions fields with the Higgs field $\Phi(x)$. This give rise to the following gauge invariant term:

$$-\mathcal{L}_Y = (Y_u)_{ij}\, \bar{Q}_{L\,i}\, u_{R\,j}\, \tilde{\Phi} + (Y_d)_{ij}\, \bar{Q}_{L\,i}\, d_{R\,j}\, \Phi + (Y_e)_{ij}\, \bar{L}_{L\,i}\, e_{R\,j}\, \Phi + h.c. \tag{2}$$

After spontaneous breaking of the $SU(2)_L x U(1)_Y$ symmetry by the vacuum expectation value of the Higgs field in the *Unitary gauge* we obtain various mass terms of the kind $m_f\, \bar{f}_L\, f_R$ with:

$$(m_f)_{ij} = \frac{v}{\sqrt{(2)}}(Y_f)_{ij} \tag{3}$$

Together with these terms in Eq. 2 we also have the flavour changing terms with the factor $\gamma^\mu W_\mu$. The difference between quarks and leptons is the way we can diagonalise the interaction and the Y matrices. We have the Y_U and Y_D term for both up-type quarks and down-type quarks that set the rotation matrix for each of them. But they are different and I can not set them to be one the inverse of the other. This give the CKM matrix in the flavour changing term. We do not have both up-type and down-type mass term for the leptons doublets since neutrinos are massless in the model and then only one of the two matrix has this constraint. We then have the liberty to set the two rotation matrices, one the inverse of the other, and then conserve three quantity from three different U(1) symmetries. We associate now these three numbers with electron, muon and tau number conservation.

Following that any additional term in the Lagrangian involving the lepton fields will allow leptons to mix and will break this conservation law. Whatever, any of this will be an extension of the Standard Model as we know it now. Possible extensions could be neutrino masses terms or an Higgs doublet.

A more extensive explanation can be found in a paper by L. Calibbi and G. Signorelli (Ref. 3), which give further details about the possible extensions and more about the other processes similar to Mu2e like $\mu^+ \longrightarrow e^+\,\gamma$ (recently studied by MEG at PSI) and $\mu^+ \longrightarrow e^+\,e^+\,e^-$ (by SINDRUM).

This is the theoretical environment: an observation of the muon conversion in an electron will violate the muon and electon number conservation law and will allow additional terms in the Lagrangian resulting in new physics beyond the Standard Model.

3 The Mu2e Experiment

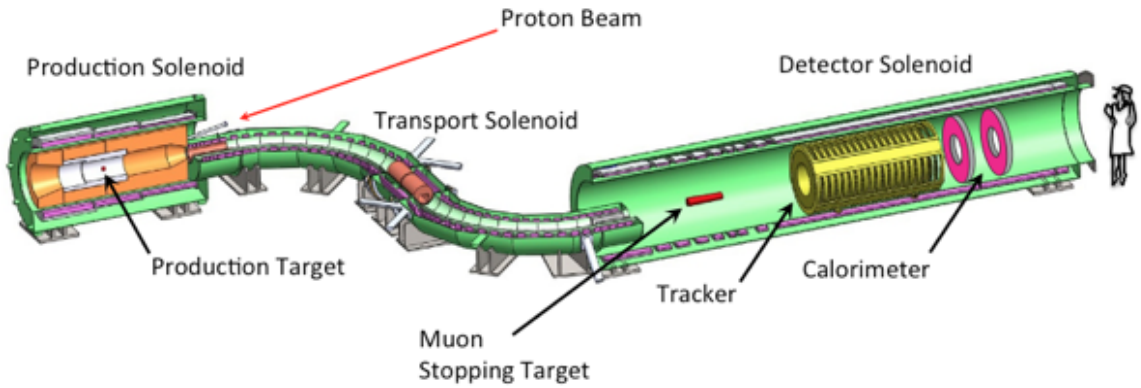

Figure 1: Schematic view of the Mu2e experiment. Muons are produced by the interactions between protons and the so-called Tungsten *Production Target*. Then the are redirected to the Transport Solenoid (TS) which reduces the background. In the end they will hit the stopping target after which we find the detector used to extract electron's signals.

Mu2e will start the search for a charged-lepton flavor violation in 2022 by measuring the events ratio:

$$R_{\mu e} = \frac{\mu^- N \longrightarrow e^- N}{\mu^- N \longrightarrow all\ muon\ captures} \tag{4}$$

The primary beam is composed of protons, that come from the Fermilab Booster with a kinetic energy on target of 8 GeV and a momentum of 8.89 GeV/c.

Muons are produced by the interactions of these protons on the *Production Target* made of Tungsten (W), they will travel trough the *Transport Solenoid* and reach the *Muon Stopping Target* where the conversion occurs. The mono-energetic (defining E_R as the recoil energy of the nucleus and B as the binding energy: $E_e = m_\mu - B - E_R$) electrons coming out from the Stopping Target can be measured with both the Tracker and the Calorimeter.

What set the design of the experiment are the rare backgrounds. We can group the contributions into three categories. I give here only a general introduction to the major background in the experiment, Ref. [**1**]. gives further explanation about these, the Transport Solenoid, the Calorimeter and the Tracker:

- Intrinsic background produced by the same muons measured in Eq.4, the major contribution comes from the so-called *decay in orbit* (DIO). This is the standard weak decay of the muon in the atomic orbit. It is then intrinsic and it scales with the number of muons and protons on each target. From 4-momentum conservation and $V - A$ theory it can be derived that the spectrum for the energy of the outgoing electron in a free-decay of a muon has an endpoint at $E_{e_{max}} = 52.8\,\text{MeV}$. But in the decay of a bound muon the spectrum is altered because the outgoing electron can exchange a photon with the nucleus. This recoil of the electron off the nucleus can make the electron's final energy equal to the conversion energy of 104.973 MeV (calculated by Czarnecki et al., Ref. [**8**]). At the endpoint, where the energy of the neutrinos are zero, the background has the same energy as the *conversion energy*. This set the energy resolution of the experiment (180 keV).

- Particles produced by the interactions between Protons and the Production target. Many particles can be produced but the two major contribution come from *radiative Pion capture*: $\pi^- N \longrightarrow \gamma N'$ (RPC) that sets a particular pulsed structure of the beam and the antiproton production. The pulsed structure is used to select a time window in which the pions have been reduced to an acceptable level and also everything that is left are muons. Even with the pulsed beam structure the RPC

background is one of the biggest challenge of the experiment because its spectrum is distorted by *radiative muon capture*: $\mu^- N \longrightarrow \gamma N' \nu_\mu$ and hard to reconstruct.

- Cosmic rays can produce interactions or decays close to the target. This background is shielded with an hermetic veto around the apparatus.

4 Antiproton background

I will now focus on the antiproton background.
Antiprotons can be produced in the Tungsten Production Target by the following reaction:

$$p + W \longrightarrow (W^* + \bar{p}) + X \tag{5}$$

Like muons, in the absence of a magnetic field, what we have is that the component produced toward the transport solenoid is the only one we are interested in. With the introduction of the magnetic field we must consider, and add, another component due to some events produced in the opposite direction but bent by the solenoid. There is actually another component that contributes to our events. Looking inside the target, some antiprotons may be produced backwards with respect to the TS but they could be scattered back and redirected towards it.

We now define two different frames that will help us describe separately the physics and implementations in the experiment:

- The *Mu2e frame* (Fig. 2) is the one that is defined by the geometry of the Production Solenoid. The frame is right-handed with the z-axis aligned with the magnetic axis of the solenoid and points towards the Transport Solenoid (TS).
- The *Xsec frame* (cross-section frame, as shown in Fig. 2) is the physical one. The incoming proton direction is the only meaningful direction for the physics so the z-axis is aligned with this direction in this frame and is always right-handed.

Following this nomenclature, antiprotons will be produced in the Xsec frame flat in ϕ and with a certain θ and p based on the cross section. These values correspond to others in the Mu2e frame but the rotation is not trivial. The two frames are simply rotated by a 14 deg angle in the Mu2e z-y plane, as shown in Fig. 2, but what is a flat ϕ dependence in the Xsec frame becomes complicated in the transformed one. We postpone the problem and focus on what calculating the production in the Xsec frame for now. These produced antiprotons can now follow the muons inside the Transport Solenoid because they have the same sign and are transported through the curved central solenoid. Because of their high momentum, some of them will not be bent sufficiently by the solenoid to follow the solenoid bend and be stopped inside it. A fraction with the correct angle and momentum can however reach the Stopping Target located in the Detector Solenoid and start the process described in Fig. 3. Inside the aluminum Stopping Target antiprotons and protons can annihilate forming pions, π_0 in particular. After the decay into γ pairs we will end up with an electron pair if the γs in exam will have enough energy. This is what we called signal and this is why we consider antiprotons a background source.
With this picture we can now focus on the production mechanism and why it is important to understand it in the best possible way.

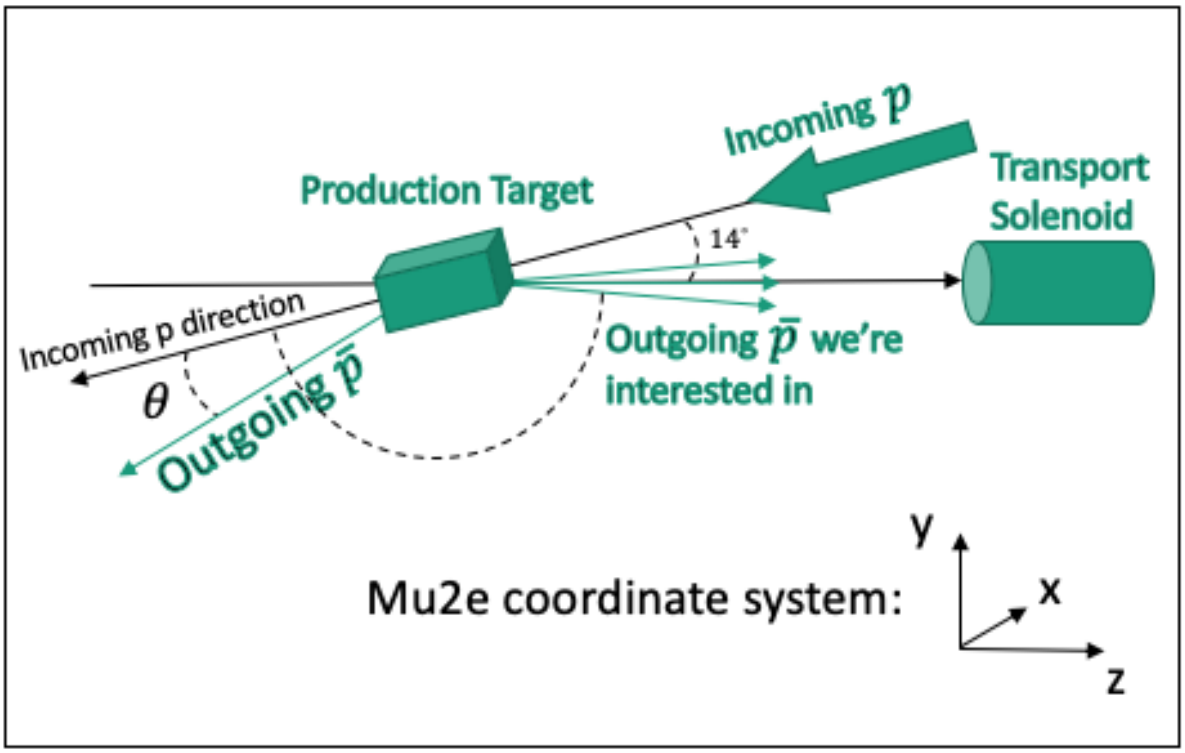

Figure 2: Explanation of the Mu2e frame and what I called "cross section" (Xsec) frame. The Mu2e frame is defined by the axis of the solenoid (the z-axis) while the Xsec frame is defined by the incoming proton direction.

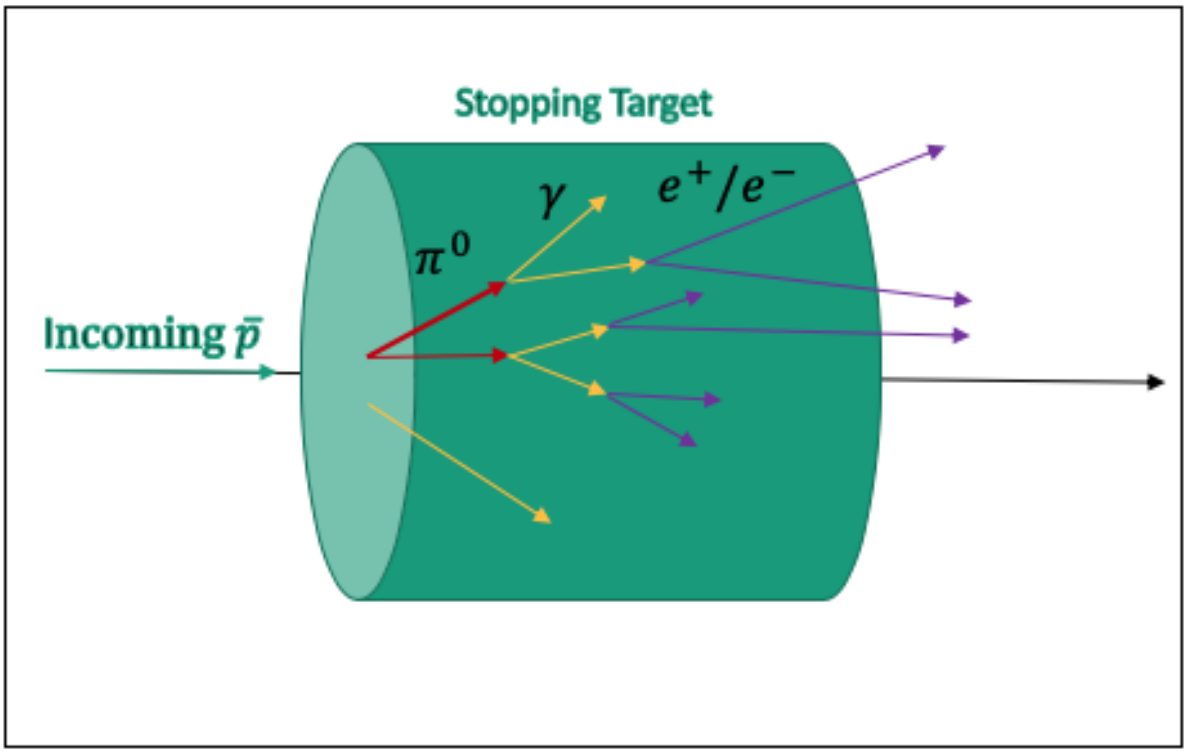

Figure 3: Schematic of the main process that contribute to the background. Antiprotons can annihilate in the stopping target and create pions which decays into 2 photons. An electron pair will then be produced if the photon has enough energy.

5 The present situation

5.1 Available data

We face now the first problem. Remembering the incoming proton energy, what we need in term of data are pW collisions (we can generalize it to proton heavy-nucleus collision) *close* to the $\bar{p}$ production threshold, which is 4.3 GeV if we include the Fermi motion in the calculation (5.1 if we do not include it). The geometry of the experiment also suggest to us that we would like to have data in the backward direction, opposite to the incoming proton, as we have seen in Fig.2.
The problem is that the majority of what we have are data at higher energies (~ 100 GeV) and mostly from forward angles in pp collisions. It is very hard to think we can extrapolate results obtained fitting these data to our problem; it could be correct but we cannot find a real reason to believe a similar behavior applies both far and close to the antiproton production threshold. And so only a small amount of cross section data are left. We will compare our model to Sergei Striganov's one, which uses these little data, and we will use the same set so we will stay comparable. The same will be for the comparison with Ying Wang's one, which is extrapolating results from high energy fitted data instead.
Fig. 4 shows the θ angles in the laboratory frame for these data points together with a legend for the following plots.
As it can be seen in the list, the backward produced data are very reduced.

Black	0
Red	3.5
Green	10.5
Blue	10.8
kRed+2	59
kYellow+2	97
kOrange	119

Figure 4: List of the angles in the LAB frame we are fitting, the same set as the one used by Striganov. A color scheme for the next plots is included.

5.2 Available models

Trying to construct a model, the physics in which we are interested can be simplified into the following reaction:

$$p + p \longrightarrow (p + \bar{p}) + p + p \tag{6}$$

This will tell us everything about the fundamental process behind Eq. 5 but is very difficult to build a model in which we describe the last equation in terms of this simpler one. Eq. 5 is thus very complicated to be described in terms of QCD and people often used different parameterizations based on some variables like transverse momentum p_T or Feynman x (Ref. [**6**]).

Striganov's fit is based on a particular parameterization of $\bar{p}$ invariant cross section in pp collision made by L. C. Tan and L. K. Ng (Ref. [**4**]) which used a new scaling variable $X_R = E^*/E^*_{max}$ while Ying Wang's fit is following the Duperray model (Ref. [**5**]).

The actual antiproton background rate calculated from these models is based on these weak assumptions and we believe we need a more physical model. Giving some physical assumptions will be easier to keep the model under control and trust its results.

6 The new proposed model

6.1 Formula and generalities

With an initial proton energy of 10 GeV, combining baryon number and charge conservation (equation 6), it is impossible to produce an antiproton with an angle $\theta > 59\,^\circ$. What could happen is that wider angles can be obtained with an interaction with an heavier multinucleon state. Like a tennis ball hitting a big truck with a multinucleon state we can imagine the right conditions to have enough energy available in the center of mass to create every momentum we want in any direction. We introduce now a function

of the outgoing antiproton's momentum and theta called the *cumulative number* η. It is defined as the number of nucleons to be hit in order to produce an antiproton with that momentum and theta. Including this the backward antiproton production at higher momentum is suppressed but still possible, the only thing required is an higher η.

Given this definition I am ready to expose our model for the invariant cross section for antiproton

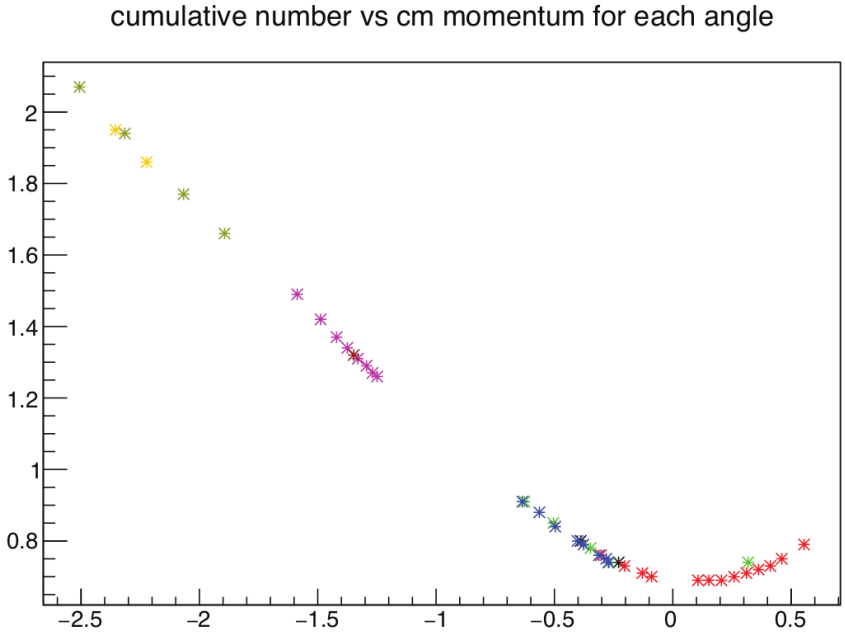

Figure 5: Cumulative number versus momentum in the center of mass [always in GeV] for all the data we have. Note that only one point really has $\eta > 2$ but it seems to follow the same shape of the others before him. Refer to Fig.4 for the color-angle legend.

production. The basic idea is to go in the center of mass and make the calculation there: if the cumulative number is less than one we fit a Gaussian with a free mean, sigma and normalization and an exponential if it is bigger than one.
The general formula is:

$$E\frac{d^3\sigma}{dp^3} = \begin{cases} N_G \dfrac{1}{\sqrt{2\pi\sigma_G^2}}\, e^{-\dfrac{|p_{cm}/p^*_{max} + O_G|^2}{2\sigma_G^2}} & \text{if cumulative number} \leq 1 \\ N_E\, S_E(\theta)\, e^{-\left|\dfrac{K_{cm}}{E^*_{max} K_{0\,cm}} + \dfrac{O_E}{E^*_{max}}\right|} & \text{if cumulative number} > 1 \end{cases} \tag{7}$$

Variables are:

- p_{cm}/p^*_{max} : Variable in the center of mass for the Gaussian term.
  where p_{cm} is defined as:
  $$p_{cm} = \begin{cases} p^{\bar{p}}_{cm} & \text{if } \cos(\theta_{cm}) \geq 0 \\ -p^{\bar{p}}_{cm} & \text{if } \cos(\theta_{cm}) < 0 \end{cases}$$
  and p^*_{max} is the maximum value of the antiproton momentum allowed by the kinematics of the Eq. 6:
  $$p^*_{max} = \sqrt{(E^*_{max})^2 - m_p^2} = \sqrt{\left(\frac{s - (3\,m_N)^2 - m_p}{2\sqrt{s}}\right)^2 - m_p^2}$$
- K_{cm} : Kinetic energy of the antiproton in the center of mass.
  $$K_{cm} = E^{\bar{p}}_{cm} - m_p$$

Free parameters are:

- N_G : Normalization for the Gaussian term
- σ_G : Sigma for the Gaussian
- O_G : Shift that determines the mean of the Gaussian
- N_E : Normalization for the Exponential term
- $K_{0\,cm}$: Shape of the Exponential in unity of E^*_{max}
- O_E : Offset for the Exponential

The cumulative number is calculated in the CM but is a Lorentz-invariant.

It is not very important what we define as center-of-mass in this model. Is possible in principle to define a new one every time based on the cumulative number and change the exponential shape following it. But, as it can be seen in Fig. 5, we have no data to fit different shapes for different cumulative numbers. We can also see that the $\eta > 2$ point seems to follow the same shape as the previous ones. It seems that, based on what we have under control, a single term $K_{0\,cm}$ will suffice. So in the model (Eq.7) the center-of-mass (CM) is always intended as the one of a proton-proton collision.

The only assumption since here is that we assume no privileged direction for antiprotons produced from ordinary matter QCD interaction. The conclusion is that we expect the cross section to be independent of the polar angle θ.

While there is no physical meaning for the Gaussian term, the exponential one is based on the so-called *Fireball* model (Ref. 10-11). The decrease in the cross-section with the outgoing kinetic energy is natural but, with this model, in case of an impact with a multi-nucleon state, we set this dependence to be exponential.

The factor $S(\theta)$ is introduced to take into account the following fact: the theta independence is in principle right if we look at the Eq. 6 but the data show a predilection for the backward direction in the center-of-mass system. Remembering that we are dealing with an heavy nucleus (Tungsten), the physics behind this can be very complicated to understand. Assuming the interaction to take place in the very first layer of the Tungsten nucleus the length of the path inside it is a function of θ_{cm} only. In case of forward produced antiproton is very unlike it can survive through the entire nucleus (which has a radius of $r_W = 6.82\,\text{fm}$ and a density $\rho_W = 2.3 \cdot 10^{14}\,\text{g/cm}^3$), so a suppression $e^{-\frac{L(\cos(\theta_{cm}))}{\lambda_I}}$ is introduced and graphically explained in Fig. 6.

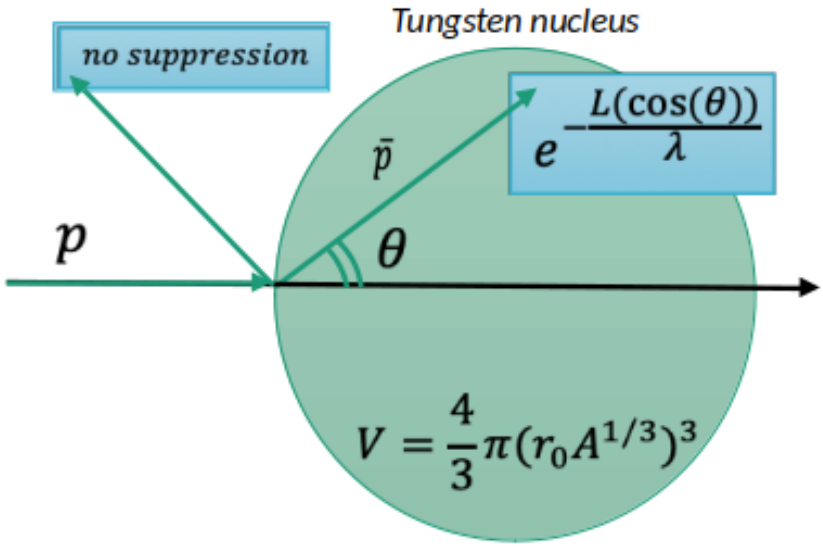

Figure 6: Graphical scheme of the forward suppression. We supposed the interaction to take place in the very first layer of the Tungsten Nucleus

Now, based on a paper by G.A. Leksin (Ref. 9), we increase the density by a factor 2^3 only when the interaction occur with a multi-nucleon state. With this change we find the nuclear interaction length λ_I to be much smaller than the Tungsten diameter only in the $\eta > 1$ case.

$$\lambda_I = 191.9\,\mathrm{g/cm^2}\,(\text{from PDG}) = \begin{cases} 1.04\,\mathrm{fm} << W_{diameter} & \text{if}\,\eta > 1 \\ 8.3\,\mathrm{fm} \sim W_{diameter} & \text{if}\,\eta < 1 \end{cases}$$

Concluding we approximate $S(\theta_{cm})$ to be constructed in such a way that the exponential part is cut off in the case of a forward production:

$$S(\theta_{cm}) = \begin{cases} 1 & \text{if}\,\cos(\theta_{cm}) \leq 0\,(\text{backward production}) \\ 0 & \text{if}\,\cos(\theta_{cm}) > 0\,(\text{forward production}) \end{cases}$$

At the moment we really do not know how to parameterize the same effect when we are dealing with a cumulative number < 1. The path inside the Tungsten and the interaction length are comparable and the problem becomes very complicated, with a lot of similarities to the neutrinos-nucleus interaction in Liquid-Argon (LAr). For now we use the parameter O_G. Without it the Gaussian would be centered at 0 and, looking at the right plot of Fig. 7, this is clearly not our case. By the way, if we think this shift to be connected with an energy loss inside the nucleus before leaving it, we have everything to answer the question. We have the interaction length, the dimensions, the density and we can extrapolate the mean energy loss with the fit and see if it is reasonable. If a refinement will be needed (despite the little data we have produced forward) this will be the direction to investigate.

Looking at the data distribution in the center-of-mass frame (right plot in Fig.7) the Gaussian and Exponential shapes seem reasonable.

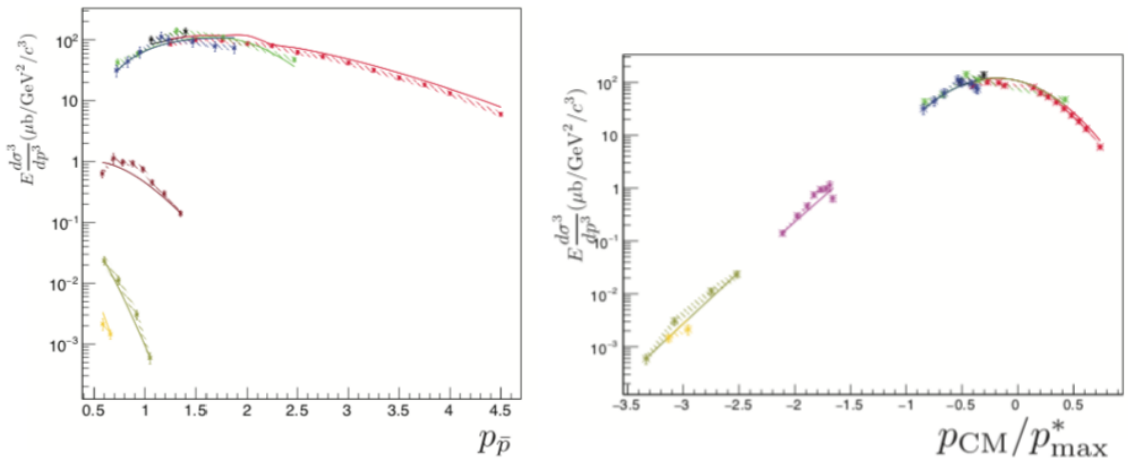

Figure 7: Invariant cross section versus laboratory momentum (left) and the natural variable for Bernstein's model p_{cm}/p^*_{max} (right). Both x-axis are in GeV/c. The fit with Eq.7 is superposed. Different angles are indicated with different colors, refer to Fig.4 for the color-angle legend.

6.2 The fit

The shown data have been fitted with the model in Eq. 7 in the same way it was done by Striganov in the old parameterization to stay comparable. That means we fitted with an initial proton Kinetic Energy of 10 GeV (Mu2e has 8.89 GeV instead). The only difference is that we included a systematic on the normalization for every different angle, due to the lack of information we have about them.

Results are shown in Fig. 8. The χ^2 is $\chi^2\,/\,d.o.f. = 88\,/\,42$ for our fit while is slightly above 1000 for Striganov's with a big contribution coming from the blue and the green points (colors do not match between the 2 plots).

The most important result we have now is the Uncertainty Matrix ready to be propagated to estimate a systematic error on the predicted antiproton rate.

I show here the fitted parameters together with a plot of the Gaussian part only, in its natural variable as explained before:
$N_G = 1.10224 \cdot 10^2$

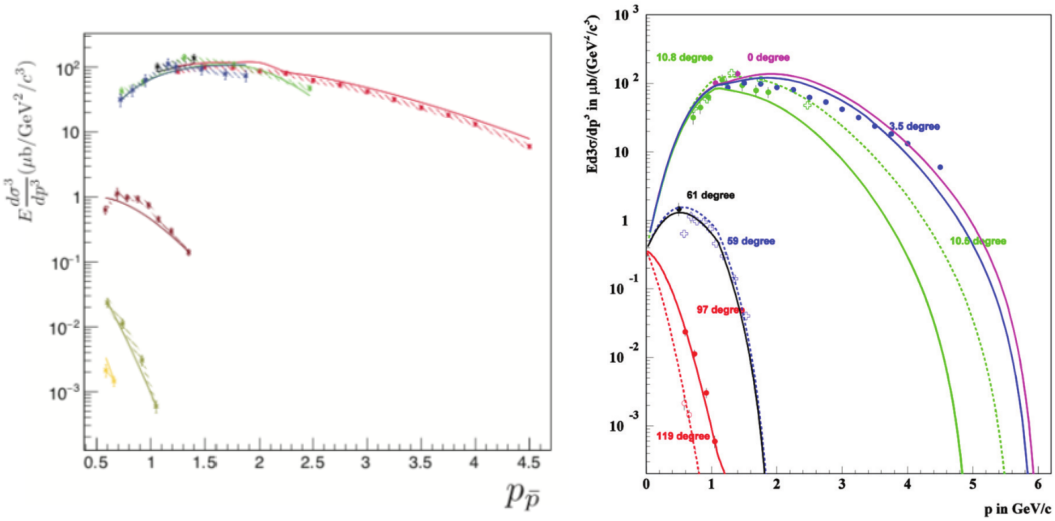

Figure 8: Fitted data both with Robert Bernstein's model (left plot) and Striganov's parameterization (right plot). Both plots show invariant cross section versus momentum of the antiproton in the laboratory frame. The calculation is done with an initial proton energy of 10 GeV (different from what we will have in Mu2e). Colors do not match between the two plots: follow the legend in Fig. 4 for ours and indications for Striganov's.

$\sigma_G = 3.65437 \cdot 10^{-1}$
$O_G = 1.76039 \cdot 10^{-1}$
$N_E = 1.94394 \cdot 10^{3}$
$K_{0\,cm} = 1.51948 \cdot 10^{-1}$
$O_E = 4.3205$

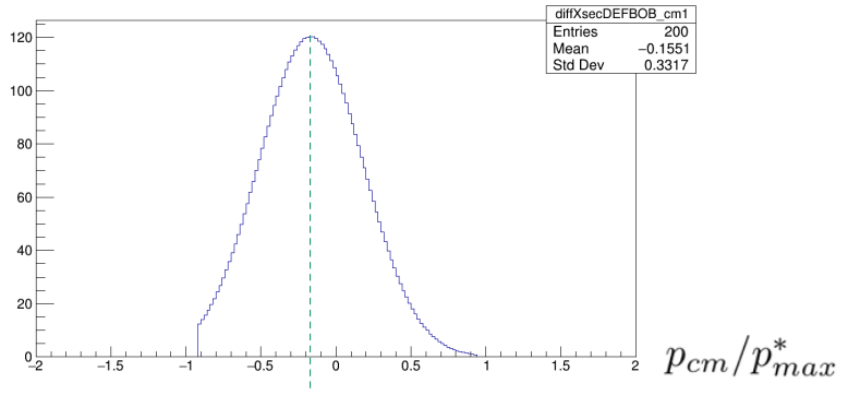

Figure 9: Gaussian term of the invariant cross section in Eq. 7 plotted with the fitted parameter. The O_G fitted shift is highlighted. Remember that p_{cm} is negative when the antiproton in backward produced and positive in the opposite case.

7 Behavior and first comparison

Now we can take a look at how the different cross sections appear. The first thing is to have an overall idea integrating over the entire phase space. I have done it setting the limits on angle and momentum based on the kinematic of the 6. I set $\phi \in [0, 2\,\pi]$, $\theta \in [0, \pi]$ and $p \in [0, 5\,GeV]$. I calculated the integral with two different techniques, just to be sure and have a double check. The first try is to loop over the entire partitioned phase space summing all the contributions weighted with the factor $p^2 \sin(\theta)$ and a factor $1\,/\,E$ in order to compensate E in the invariant cross section. Then the integral will appear as the

following sum:

$$I = 2\,\pi \left(\sum_{p=0}^{5} \sum_{\theta=0}^{\pi} \left(E\,\frac{d^3\sigma}{dp^3} \right) \frac{1}{E}\,p^2\,\sin(\theta)\,\Delta p\,\Delta\theta \right)$$

The second method is to pass through a Monte Carlo; I generated points inside a (p,θ, Y) cube, saved only the points in which $Y < E\,\dfrac{d^3\sigma}{dp^3}$ and then normalized to the total number of points.

The two methods ends with the same results of:
$I_{Bernstein} \simeq 99\,\mu b$
$I_{Striganov} \simeq 30\,\mu b$
$I_{Wang} \simeq 42\,\mu b$
The order of magnitudes seems comparable. What really interested us at a further level of precision is a comparison made *bin by bin* over the phase space. I will first show a comparison in the laboratory frame to have a first impression and then I will show the three different cross section in the center-of-mass frame that is the one in which the physics occurs.

7.1 Laboratory frame

Here in Fig. 10 we have a better overview of the overall agreement. Nothing is quantitative but the decrease at higher p_{lab} and at higher θ is reasonable.

Way more interesting is a quantitative comparison made with a ratio between them. First of all there is no reason to compare them over the entire phase space because of some obvious kinematic limits. The cross section decrease very fast with the cumulative number η falling rapidly to zero. In the calculation code there is a statement that set the cross section to zero if η is bigger than 10, so I have excluded that region from the ratio. I also excluded all the phase space region resulting in a cross section such that:

$$\underbrace{3.6 \cdot 10^{20}}_{\text{Total number of } p \text{ in Mu2e}} \quad \times \quad \mathrm{P}[p + p \longrightarrow (p + \bar{p}) + p + p] \quad \times \quad \underbrace{10^{-5}}_{\text{Probability of an } \bar{p} \text{ making an } e} \quad \geq 1$$

We require the probability resulting from the cross section to be high enough to make at the end at least 1 electron that contributes to the background. I have taken the probability of an antiproton making an electron to be $\sim 10^{-5}$, the assumption is based on a Robert H. Bernstein previous analysis (unpublished).

With this requirements the phase space is reduced as shown in Fig. 11. We are now ready to look at the ratio between the different cross sections. I decided to show here three ratio plots: Striganov over Bernstein and Ying Wang over the remaining two, shown in Fig. 12. It is important to point out that the region we are really interested in is between 0 GeV/c and 1 GeV/c in p_{lab} with a special attention to backward production (in the laboratory frame this is toward the Mu2e Transport Solenoid). This window in momentum is determined by the acceptance of the entire Transport Solenoid (relation is $p \propto B\,\rho$), antiprotons with an higher momentum will be bend less through it and end leaving the tunnel. Striganov explicitly told us to ignore what he extrapolated at higher p_{lab}, where the agreement fails, because he artificially fitted that region.

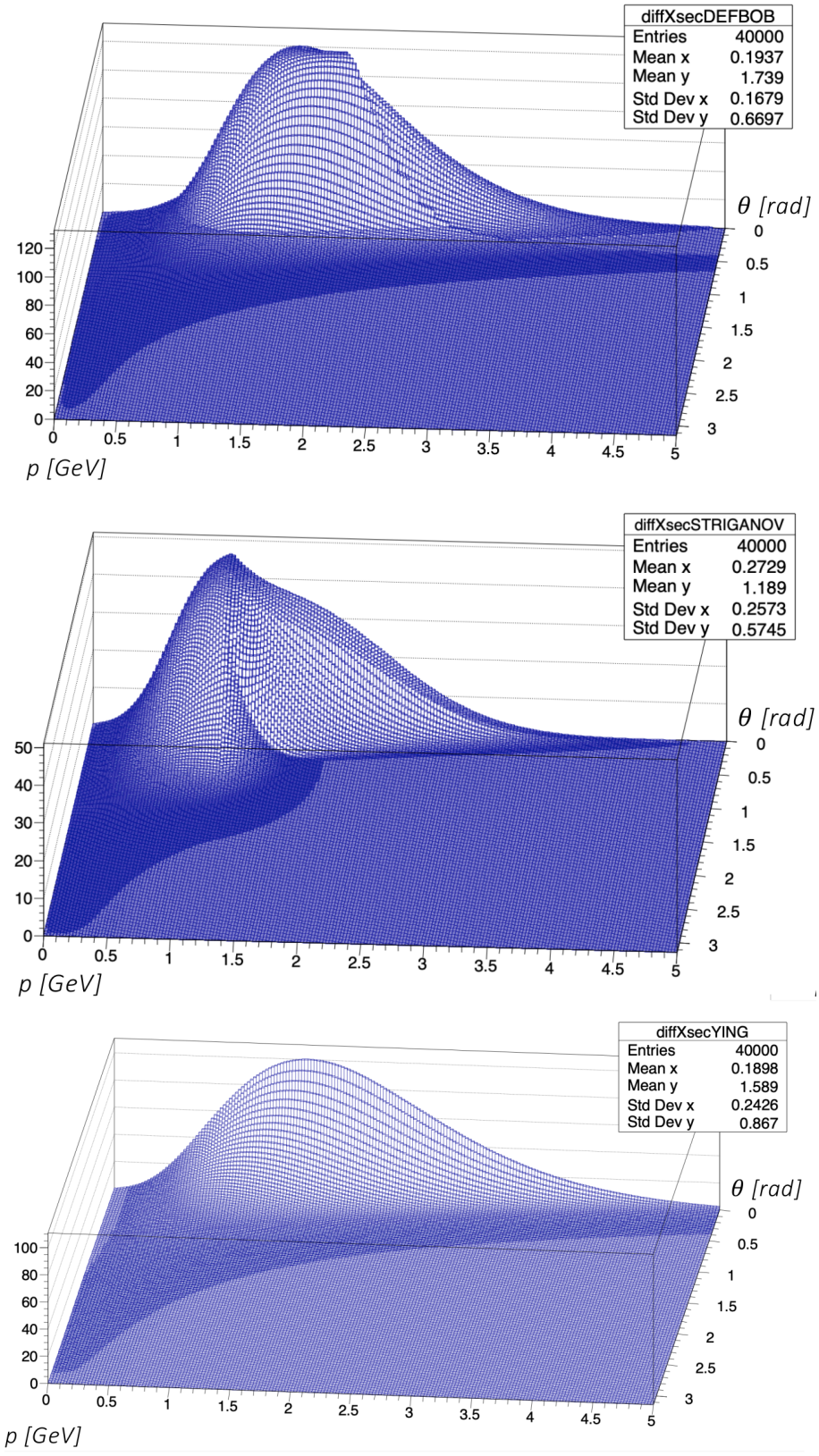

Figure 10: 2D plot of each cross section. The x-axis and the y-axis show the momentum and θ of the antiproton in the laboratory frame while on the z-axis the invariant cross section is shown. On top I am showing the result of Bernstein's new cross section model. A discontinuity is visible in that cross section caused by the definition of p_{cm} (look after Eq. 7). We defined p_{cm} in such a way and we add O_G before make the absolute value, after the boost to the lab frame this will ends with a discontinuity even if is continuous in the center-of-mass. Then, proceeding downwards, I show the cross section based on Striganov's and Ying Wang's parameterization.

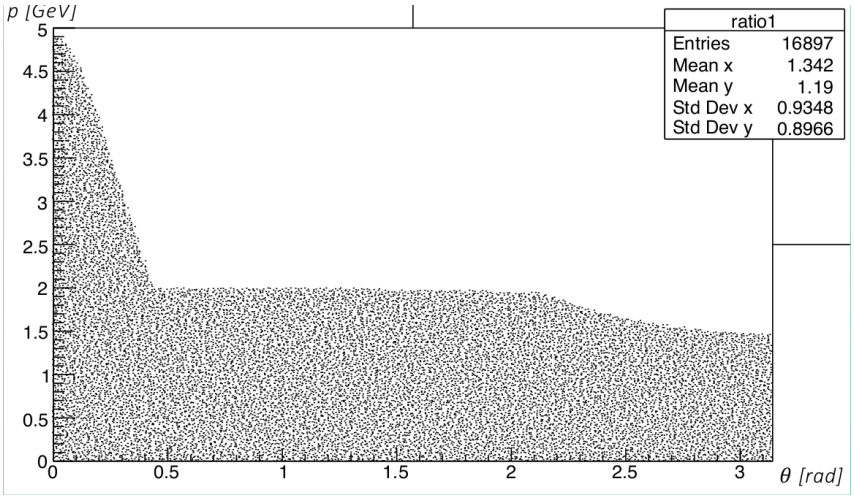

Figure 11: The plot shows the reduced phase space after the two cuts explained in the text. In the majority of the cases (in the majority of the possible angles) the probability is very small at high cumulative number. This often makes the second cut included in the first one

7.2 Center-of-mass frame

If we take a look in the center-of-mass we can deduce some information about the physics behind the process and check the validity of the assumptions we are making. The three functions are shown in Fig. 13. The first function on top, representing Bernstein's cross section, may seem discontinuous but actually the variables on x-axis and y-axis are strongly correlated in such a way that p_{cm} can not be negative in a region $\theta_{cm} < 90°$ and can not be positive while $\theta > 90°$ as well. In fact if we plot the 1D function in p_{cm}/p^*_{max} we see it as a continuous function as it must be. The other two plots represent the same cross section versus center of mass variables p_{cm} and θ_{cm} but obtained with the other two parameterizations.

We talked about the introduction of the shift O_G in order to have a better fit. I would like to emphasize now how much this is visible here. Without this shift the first plot in Fig. 14 will be symmetric with respect to $p_{cm} = 0$ and most important flat in θ_{cm}. I also noticed a similar θ dependence for Striganov's and Ying Wang's plot, in the sense that they also show a preference for the backward production and this increase our suspects.

Percentage in the total integral produced opposite to the initial proton direction:
Bernstein: 83.6 %
Striganov: 91.5 %
Ying Wang: 69.5 %

Except for this, both Striganov's and Ying Wang functions decrease with momentum, which is again reasonable in the center-of-mass.

8 The Simulation

Everything converge in a simulation performed in order to obtain an estimate of the antiproton flux at the Transport Solenoid.

I am using for it a certain amount of simulated protons hitting the Tungsten production target with a momentum distribution peaked around 8.89 GeV (Mu2e proton beam). In the center-of-mass every one of these protons produces an antiproton flat in p_{cm} and θ_{cm}; not weighted yet with any cross section.

Every antiproton event is required in this simulation by GEANT to reach the Transport Solenoid (to be precise at the virtual detector VD92 with no material between VD91 and 92, which is 1 mm downstream) and many effect I will discuss can contribute. This ends with $3 \cdot 10^8$ events generated.

My final goal was here to weight these events with the different cross sections I have discussed before and make a comparison.

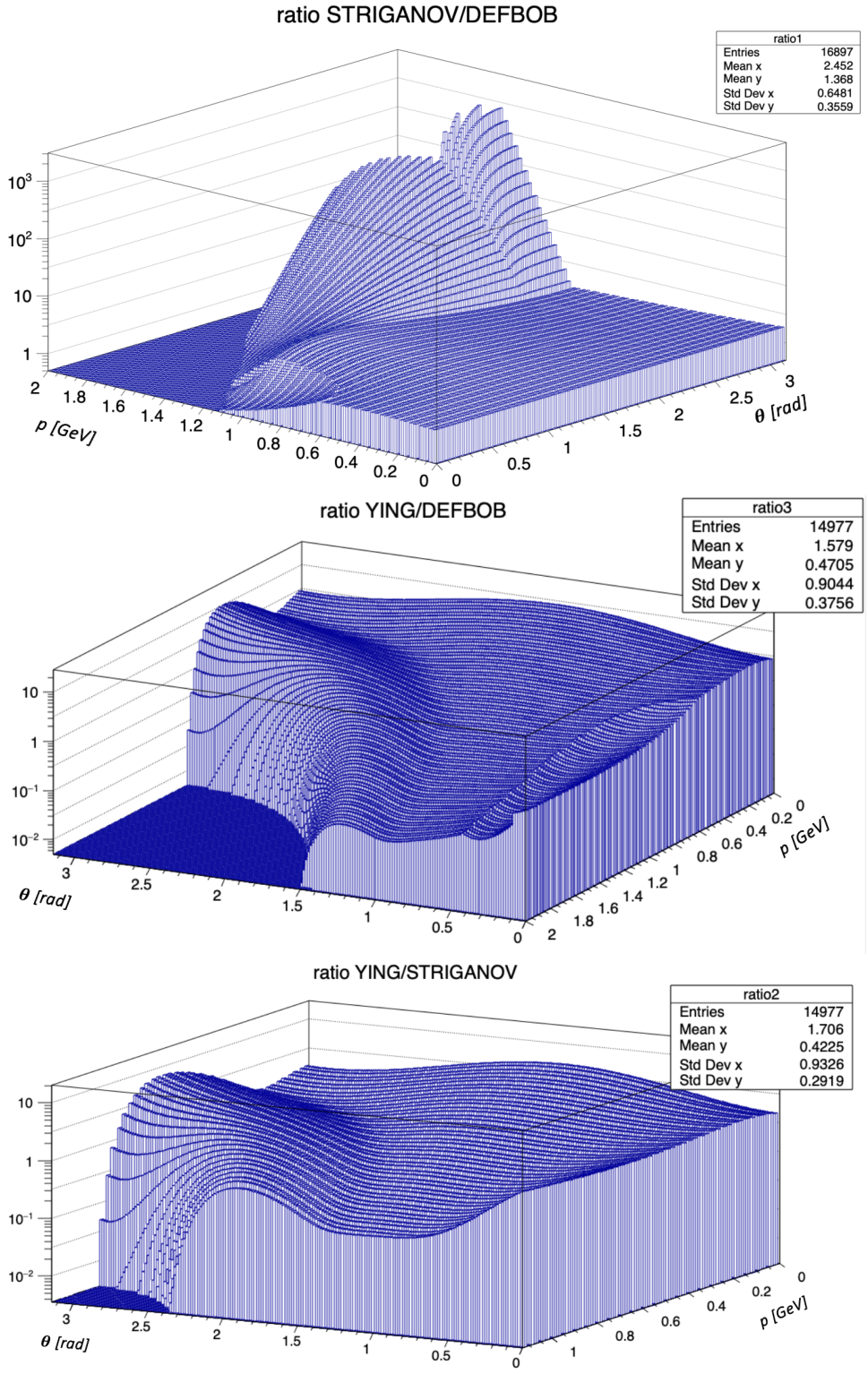

Figure 12: A version of the three ratio plot with a focus on the phase space region accepted by the cuts and an additional zoom on the region we are interested in. On the x-y plane we have the momentum and θ in the laboratory frame of the produced antiproton, the ratio is on z-axis. The first plot on top shows us an agreement in shape between Striganov's parameterization and Bernstein model (called DEFBOB in the titles). The shape agreement is distributed over the entire region between [0,1] GeV in momentum for every angle with a ratio between ~ 1 and ~ 3. The other two looks similar because of this agreement.

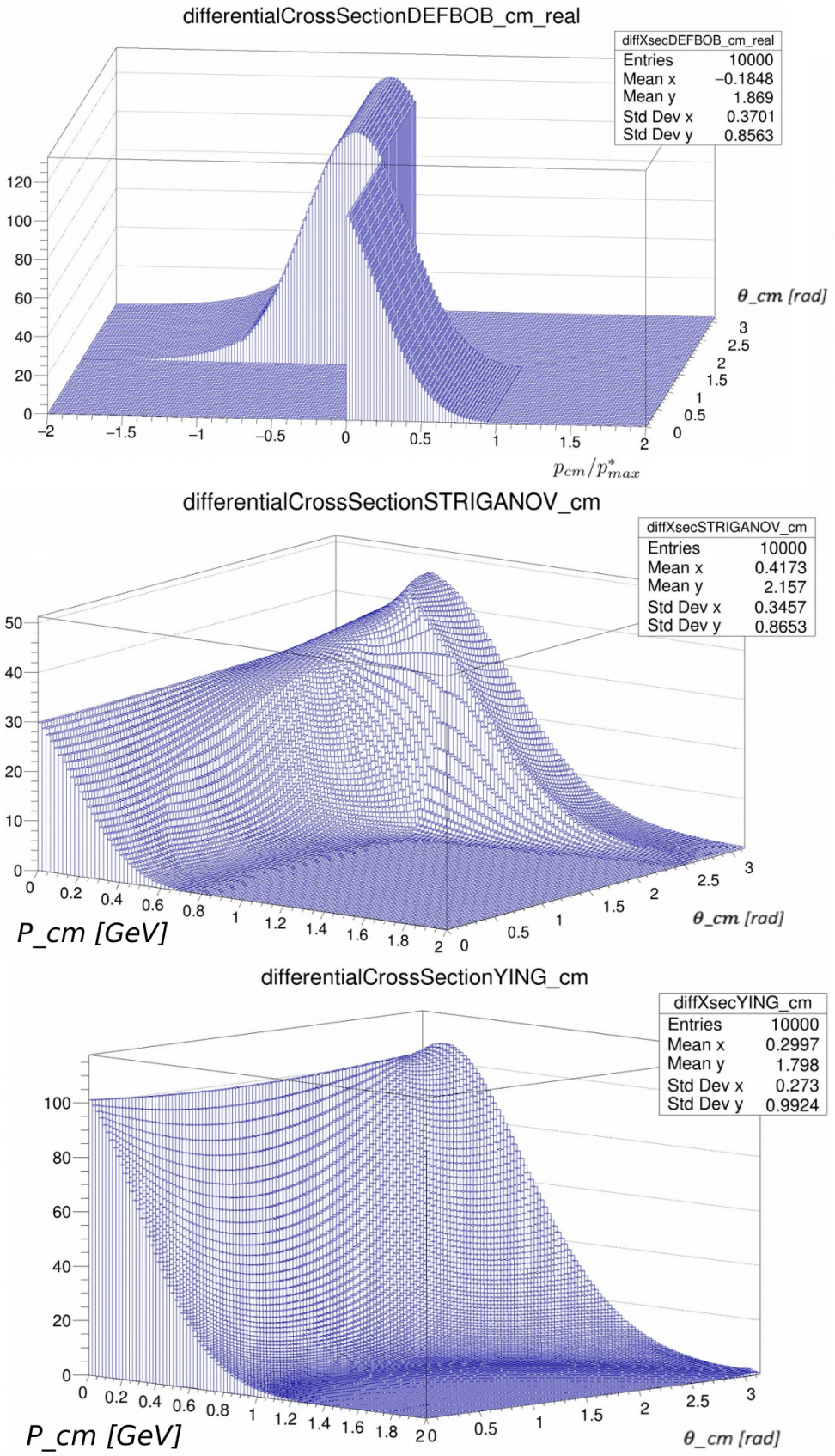

Figure 13: 2D plots for each models in the center-of-mass variables. The first plot on top represent Bernstein's cross section plotted versus his natural variables p_{cm}/p^*_{max} and θ_{cm} exactly as they are defined above in Eq. 7. This function is not discontinuous but actually not defined in the two empty regions.

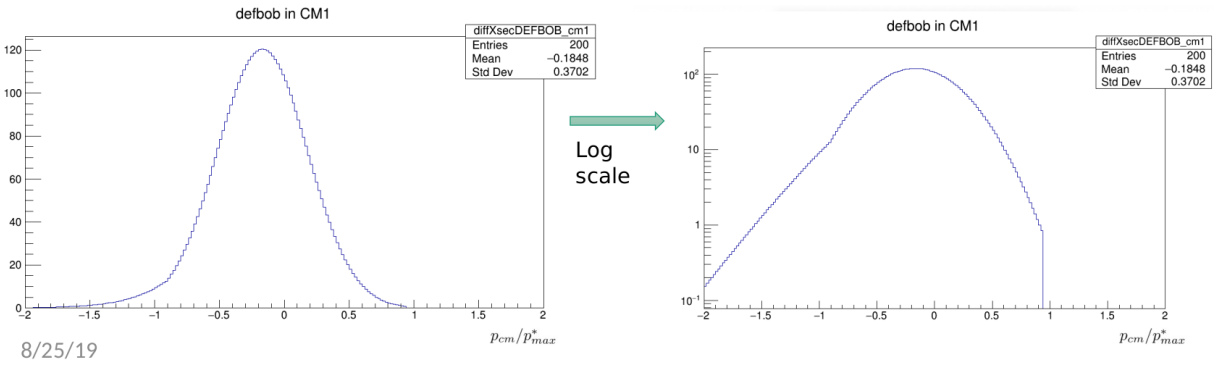

Figure 14: 1D plot for Bernstein's model. This is just a projection of the first plot of Figure 13. The log scale enhance the transition between the Gaussian region and the exponential region. Toward negative p_{cm} the exponential is permitted; towards negative p_{cm} the exponential is suppressed as explained earlier. Following the physics we should continue plotting the Gaussian term in this region, this is just a bug of the model.

8.1 Unweighted distributions and different contributions

Before weight the events it is convenient to take a look at the unweighted distributions to highlight every effect discussed in Section 4 that can contribute to direct the produced antiprotons at the entrance of the Transport Solenoid (TS).

In Fig. 15 I show the distribution of these events in the cosine of the angle θ_{Xsec} at the time of the production. I show this first because it is the physical one. In the Xsec frame (as it is defined in Section 4) $\cos\theta_{Xsec} \simeq -1$ (not = because of the 14° rotation of the Production Target, which is included in the simulation) contains all the events produced directly toward the TS. This includes the majority of the events and, recalling that we are still not weighting with cross section, it is straightforward to understand why they do not need any further physical effect to get inside. The distribution decrease until $\cos\theta_{Xsec} \simeq 1$. These events are produced in the opposite direction with respect to the TS but they can reach it thanks to the magnetic field or interactions inside the target and be scattered back. This contribution is far lower than anything else but a certain fraction is still appreciable. The effect of the 14° is also visible in Fig.15 from the little plateau at the beginning and the ascent at the very right. Without this little rotation the distribution will be monotone.

If we make the transformation to the "Mu2e frame" the distribution looks like what I show in Fig. 16. The shape is the same, without the 14° (which makes the transformation not trivial) this will just be a reflection with respect to 0. Since we are just changing the frame coordinates the physics contributions are the same as before.

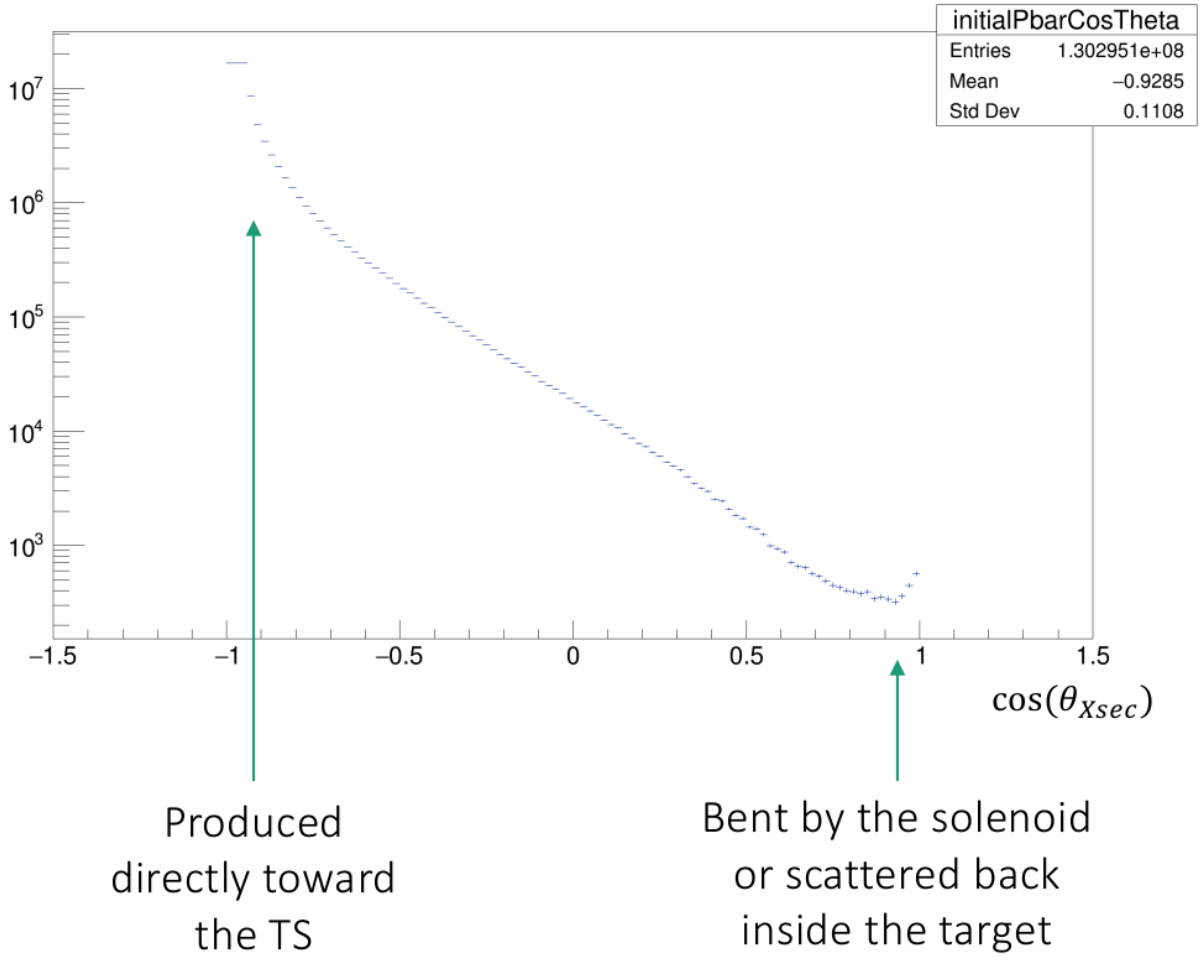

Figure 15: The plot shows a distribution of the simulated events in the cosine of the initial θ angle defined with respect to the Xsec frame as defined in Section 4. Every event is required to reach the Transport Solenoid, we see here how they are distributed in the angle at the time of the production. In the Mu2e frame. The two regions are explained in the Figure.

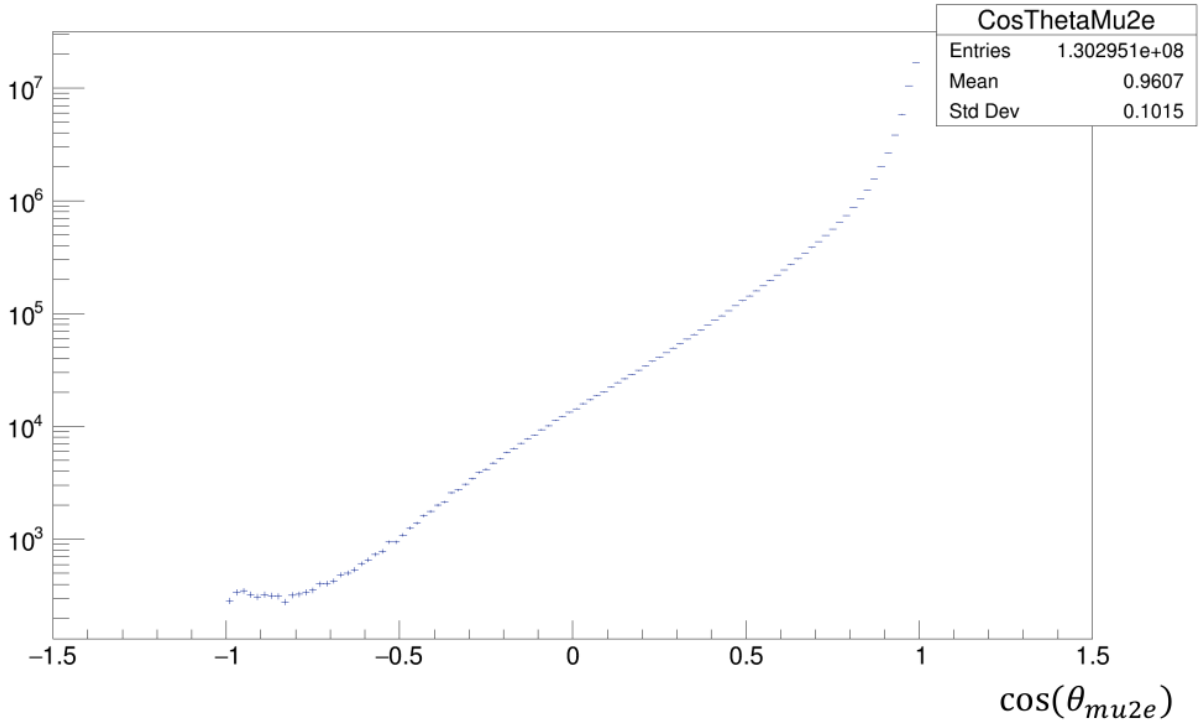

Figure 16: Distriution of the simulated events in the cosine of the initial θ defined with respect to the Mu2e frame (defined in section 4, z axis pointed alog the magnetic axis of the Production Solenoid).

9 Weighted distributions

9.1 Uncertainties

Together with $\cos\theta$ every event has a momentum $p_{\bar{p}}$ at the time of the production. We integrate over it when I showing the $\cos\theta$ distributions. This means that we fill the bins independently of the momentum of the antiproton. At this level the y-axis is then the sum over the entries with different p in a fixed $\cos\theta$ bin:

$$Y(cos\theta_{bin}) = \sum_{i=1}^{n_p(cos\theta_{bin})} 1 \tag{8}$$

Where $n_p(cos\theta_{bin})$ means the total number of accepted antiprotons at that fixed $\cos\theta_{bin}$ independently of $p_{\bar{p}}$.

If now I weight every event with the corresponding cross section Eq. 8 will be modified into:

$$Y(cos\theta_{bin}) = \sum_{i=1}^{n_p(cos\theta_{bin})} \alpha_i \tag{9}$$

Where the $\alpha_i(p_{\bar{p}}, \theta_{\bar{p}}, p_p)$ are the weights and they can come from different models.

As I mentioned the most important new comes with Bernstein's model is the uncertainty matrix on the fit parameters. This will propagate through the calculation of the cross section and consequently the weight. The formula for the uncertainty on the α_i is the usual one with $p\prime$ and $q\prime$ running over the fit parameters k:

$$\sigma^2_{\alpha_i} = \sum_{p\prime,q\prime} \frac{\partial\alpha_i}{\partial k_{p\prime}} \frac{\partial\alpha_i}{\partial k_{q\prime}} cov_{k_{p\prime}k_{q\prime}} \tag{10}$$

Looking at the Eq. 9 there are two contributions to the total uncertainty. First the statistical error ($\sim \sqrt{n_p}$) but is managed and added correctly over n_p by ROOT (with the use of Sumw2()). The second contribution is the systematic uncertainty coming from our knowledge of the model, which translates to the uncertainty of the fit parameters. Then what we need is a good estimator for:

$$\sigma^2_Y = \sum_{p,q} \frac{\partial Y}{\partial k_p} \frac{\partial Y}{\partial k_q} cov_{k_pk_q} = \sum_{p,q} \frac{\partial \sum_i \alpha_i}{\partial k_p} \frac{\partial \sum_j \alpha_j}{\partial k_q} cov_{k_pk_q} \tag{11}$$

$$= \sum_{p,q} \sum_{i=j} \frac{\partial \alpha_i}{\partial k_p} \frac{\partial \alpha_j}{\partial k_q} cov_{k_p k_q} + \sum_{p,q} \sum_{i \neq j} \frac{\partial \alpha_i}{\partial k_p} \frac{\partial \alpha_j}{\partial k_q} cov_{k_p k_q}$$

The calculation for the first term of the sum is easy to be implemented in a ROOT macro but for the second one needs to be able to access α_i and α_j not separately (as it is for the first term) but simultaneously in the same iteration over the events. I did not have the time during the internship to find a way to implement the right formula and I decided to estimate σ_Y^2 with:

$$\hat{\sigma}_Y = \sum_{i=1}^{n_p(cos\theta_{bin})} \sigma_{\alpha_i} \tag{12}$$

Is it possible to demonstrate that this will overestimate Eq. 11 (demonstration is attached at the end) but has a lot of main advantages: is very easy to implement, fast to compute and will give us a good enough estimate (as it can be seen in the weighted distribution, Fig. 17). In any case, when dealing with backgrounds, it is always better to be conservative. In that sense an overestimate of the error, if not too big, is not that bad.

9.2 Comparison between models

Final results for the weighted distributions are shown in Fig. 17. Every event has been weighted with all the three available models and been shown on the same plot. Blue points come from Bernstein's weights, reds from Striganov's and yellows from Ying Wang's. Uncertainties for Bernstein's are treated as I said before in Section 9.1; we do not have any information about the errors on the parameterization for the other two and so uncertainties are not shown. The numbers on the y-axis indicates the number of

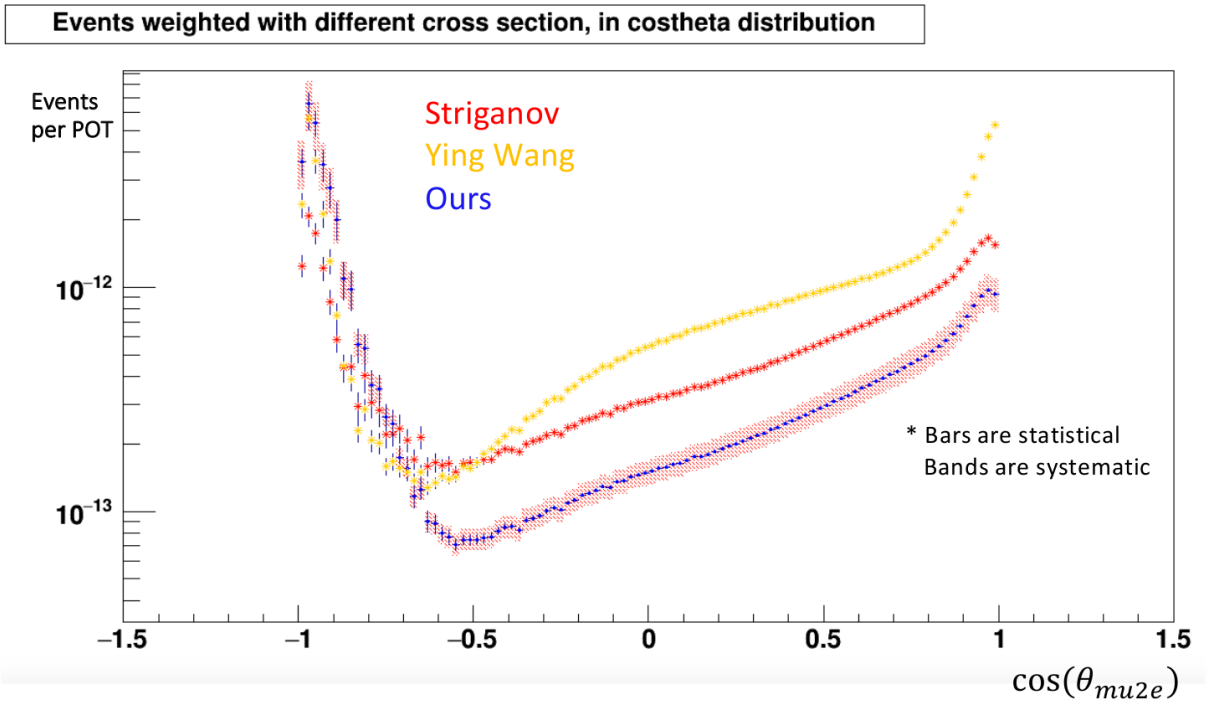

Figure 17: Final weighted distribution of events per Proton on Target (POT) in the cosine of the production angle θ in the Mu2e frame. Multiply the y-axis by the total number of p in Mu2e will give you the total number of $\bar{p}$ produced at that $cos\theta_{bin}$). Every event here, as before, is required to reach the TS, we are looking here at the distribution in θ at the time of the production. *-1 events* are weighted with an higher cross section than *+1 events* because the first are forward produced in the physical (Xsec) frame. Blue points come from Bernstein's weights, reds from Striganov's and yellows from Ying Wang's. We do not have any information about the uncertainties for the two other parameterizations. For Bernstein's model statistical error is indicated with bars and the bands represent the systematic estimated with Eq. 12.

events per "Proton On Target" (POT). It means that to obtain the total number of antiprotons reaching the TS coming from that bin in $\cos\theta$ you have to multiply by $3.6 \cdot 10^{20}$, which is the total number of expected protons on target in the entire Mu2e experiment. An integral over the bins in $\cos\theta$ will give the

total number of antiprotons reaching the TS. This number is not the goal of this work because it will be decreased a lot when these events will be propagated inside the TS and through the Stopping target. The interesting number is the number of electrons obtained at the end.

We next compare Fig. 17 with the unweighted one (Fig. 16). The left side of the plot is now raised by the big forward cross section (remember that ~ -1 for $\cos\theta_{Mu2e}$ in forward production in Xsec frame). If everything is done correctly we end with this consideration: in the Xsec frame forward events are favored with an high cross section but they need physics like magnetic field and scattering to reach the TS while backward events are disadvantaged from the production point of view but for them is very easy to gets into the TS that is directly in front. The two cases seems to be comparable at the end within a factor ~ 10 at maximum.

Is interesting to see that, based on the uncertainty, the new model predicts a different rate from the previous one (which is Striganov's one), a factor ~ 2 lower on the right and about the same factor (hard to say because of the uncertainties) on the left. We know, from a previous simulation, that after the propagation inside the TS, the majority of the total flux will come from the right side of this plot and so if everything is right we are predicting now a lower background contribution coming from antiprotons.

The uncertainties of the order of $\sim 10\%$ also tell us how much precision will be required in the construction of an hypothetical collimator shield inside the TS. At the moment the construction is under discussion, it might be not worth building (also placing it inside the TS is quite expensive) and is probably possible to have the same effect with a reduction of the diameter of the entrance window of the TS (with no significant loss on the muon flux). But for sure an understanding of the uncertainty is crucial to face this problem.

Is even more interesting to take a look at the same plot but with a cut in the antiproton momentum at the entrance of the TS (Fig. 18). This cut in momentum will reject the events far from the acceptance of the TS. Nothing is changed in the left region, and this is understandable, because they also had the

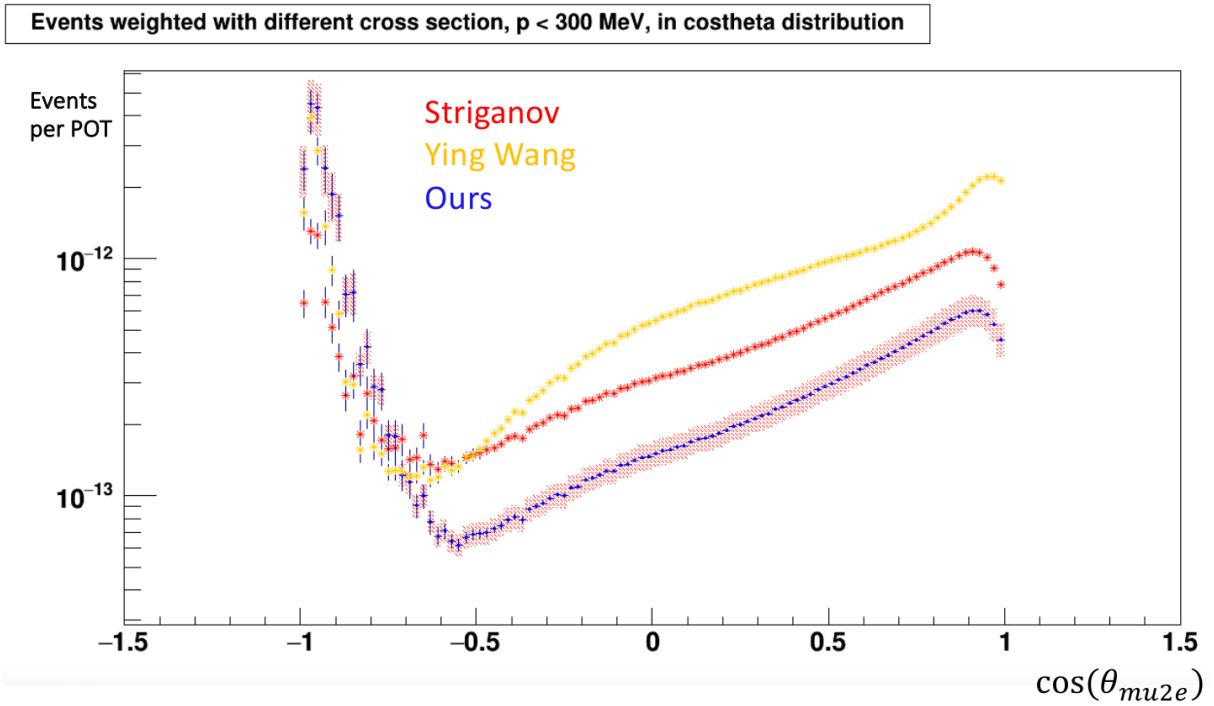

Figure 18: Same plot as Fig. 17 but with a cut in the momentum the antiproton has when he reach the TS. The cut is set at 300 MeV to reject the events outside the acceptance of the TS.

same momentum in the previous plot. In order to be bent or scattered back they need a small initial momentum that will result in again a small momentum at the TS. Some differences appear in the very right side of the plot, Events can be produced directly in front of the TS with any momentum allowed by the cross section and so we expected a decrease here after the cut, which is confirmed.

10 Appendix A: Overestimation of the uncertainty

I want to estimate:

$$\sigma_Y^2 = \sum_{p,q} \frac{\partial Y}{\partial k_p} \frac{\partial Y}{\partial k_q} cov_{k_p k_q} = \sum_{p,q} \frac{\partial \sum_i \alpha_i}{\partial k_p} \frac{\partial \sum_j \alpha_j}{\partial k_q} cov_{k_p k_q}$$

$$= \sum_{p,q} \sum_{i=j} \frac{\partial \alpha_i}{\partial k_p} \frac{\partial \alpha_j}{\partial k_q} cov_{k_p k_q} + \sum_{p,q} \sum_{i \neq j} \frac{\partial \alpha_i}{\partial k_p} \frac{\partial \ \alpha_j}{\partial k_q} cov_{k_p k_q}$$

with:

$$\hat{\sigma}_Y = \sum_i^{n_p(cos\theta_{bin})} \sigma_{\alpha_i}$$

$$\hat{\sigma}_Y^2 = (\sum_i \sigma_{\alpha_i})^2 = \left(\sum_i \sqrt{\sum_{p\prime,q\prime} \frac{\partial \alpha_i}{\partial k_{p\prime}} \frac{\partial \alpha_i}{\partial k_{q\prime}} cov_{k_{p\prime} k_{q\prime}}} \right)^2$$

$$= \sum_{p,q} \sum_{i=j} \frac{\partial \alpha_i}{\partial k_p} \frac{\partial \alpha_j}{\partial k_q} cov_{k_p k_q} + \sqrt{\sum_{p\prime,q\prime} \frac{\partial \alpha_i}{\partial k_{p\prime}} \frac{\partial \alpha_i}{\partial k_{q\prime}} cov_{k_{p\prime} k_{q\prime}}} \sqrt{\sum_{p\prime,q\prime} \frac{\partial \alpha_j}{\partial k_{p\prime}} \frac{\partial \alpha_j}{\partial k_{q\prime}} cov_{k_{p\prime} k_{q\prime}}}$$

The first term in the sum is the same for the sigma and for estimator so if I want to show that $\hat{\sigma}_Y \leq \sigma_Y^2$ I only need to demonstrate that

$$\sqrt{\sum_{p\prime,q\prime} \frac{\partial \alpha_i}{\partial k_{p\prime}} \frac{\partial \alpha_i}{\partial k_{q\prime}} cov_{k_{p\prime} k_{q\prime}}} \sqrt{\sum_{p\prime,q\prime} \frac{\partial \alpha_j}{\partial k_{p\prime}} \frac{\partial \alpha_j}{\partial k_{q\prime}} cov_{k_{p\prime} k_{q\prime}}} \geq \sum_{p,q} \sum_{i \neq j} \frac{\partial \alpha_i}{\partial k_p} \frac{\partial \ \alpha_j}{\partial k_q} cov_{k_p k_q}$$

We can see each term as a scalar product with the covariance matrix as the metric. This simplify the notation and brig us to:

$$\sqrt{\partial \alpha_i \cdot \partial \alpha_i} \sqrt{\partial \alpha_j \cdot \partial \alpha_j} \geq \partial \alpha_i \cdot \partial \alpha_j$$

This leads us to the famous Schwarz inequality:

$$|\partial \alpha_i| \, |\partial \alpha_j| \geq \partial \alpha_i \cdot \partial \alpha_j$$

References

[1] R.H. Bernstein (2019), The Mu2e Experiment, Front, Phys, 7:1, doi: 10.3389/fphy.2019.00001.

[2] R.H. Bernstein and P.S. Cooper (2014), Physics Reports C, Charged Lepton Flavor Violation: An Experimenter's Guide.

[3] L. Calibbi and G. Signorelli (2017), Invited review for La Rivista del Nuovo Cimento, Charged Lepton Flavour Violation: An Experimental and Theoretical Introduction.

[4] L.C. Tan, L.K. Ng (1983), Journal of Physics G: Nuclear Physics 1983, Vol.9, N.10, p. 1289, Parametrization of $\bar{p}$ invariant cross section in p-p collisions using a new scaling variable, Also available as mu2e-docdb 8403.

[5] R.P. Duperray et al. (2008), Parameterization of the antiproton inclusive production cross section on nuclei, Also available as mu2e-docdb 8403.

[6] F.E. Taylor et al. (1975), Physical Review D, Vol.14, N.5, Analysis of radial scaling in single-particle inclusive reactions, Also available as mu2e-docdb 8403.

[7] J.R. Letaw, R. Silberberg and C.H. Tsaoal. (1983), Proton-nucleus total inelastic cross section: an empirical formula for $E > 10\,GeV$, Also available as mu2e-docdb 8403.

[8] Czarnecki A, Garcia i Tormo X, Marciano WJ, Phys Rev D (2011) 84:013006, Muon decay in orbit: spectrum of high-energy electrons, doi: 10.1103/PhysRevD.84.013006

[9] G. A. Leksin (2002), Methods for Investigating Nuclear Matter under the Conditions Characteristic of Its Transition to Quark–Gluon Plasma

[10] Yu. T. Kiselev, V. A. Sheinkman et al., Phys Rev C (2012) 85:054904, Probing of compact baryonic configurations in nuclei in A(p,p^-)X reactions and antiproton formation length in nuclear matter. Available at arXiv:1204.2669

[11] S.S. Shimanskiy (2014), Cumulative processes out off the nucleus fragmentation region. Available at arXiv:1411.7211